
AFRL-AFOSR-VA-TR-2016-0279

# Preliminary Work for Identifying and Tracking Combustion Reaction Pathways by Coherent Microwave Mapping of Photoelectrons

**Zhili Zhang**
**UNIVERSITY OF TENNESSEE KNOXVILLE TN**

**06/24/2016**
**Final Report**



Air Force Research Laboratory
AF Office Of Scientific Research (AFOSR)/ RTA1
Arlington, Virginia 22203
Air Force Materiel Command

# REPORT DOCUMENTATION PAGE

*Form Approved*
*OMB No. 0704-0188*



| 1. REPORT DATE *(DD-MM-YYYY)* | 2. REPORT TYPE | 3. DATES COVERED *(From - To)* |
|---|---|---|
| 30-07-2016 | Final Performance | 15 Sep 2014 to 14 Mar 2016 |

**4. TITLE AND SUBTITLE**
Preliminary Work for Identifying and Tracking Combustion Reaction Pathways by Coherent Microwave Mapping of Photoelectrons

**5a. CONTRACT NUMBER**

**5b. GRANT NUMBER**
FA9550-14-1-0329

**5c. PROGRAM ELEMENT NUMBER**
61102F

**6. AUTHOR(S)**
Zhili Zhang

**5d. PROJECT NUMBER**

**5e. TASK NUMBER**

**5f. WORK UNIT NUMBER**

**7. PERFORMING ORGANIZATION NAME(S) AND ADDRESS(ES)**
UNIVERSITY OF TENNESSEE KNOXVILLE TN
1331 CIR PARK DR
KNOXVILLE, TN 37916-3801 US

**8. PERFORMING ORGANIZATION REPORT NUMBER**

**9. SPONSORING/MONITORING AGENCY NAME(S) AND ADDRESS(ES)**
AF Office of Scientific Research
875 N. Randolph St. Room 3112
Arlington, VA 22203

**10. SPONSOR/MONITOR'S ACRONYM(S)**
AFRL/AFOSR RTA1

**11. SPONSOR/MONITOR'S REPORT NUMBER(S)**
AFRL-AFOSR-VA-TR-2016-0279

**12. DISTRIBUTION/AVAILABILITY STATEMENT**
A DISTRIBUTION UNLIMITED: PB Public Release

**13. SUPPLEMENTARY NOTES**

**14. ABSTRACT**

This report summarizes our efforts during Sep. 15th 2014 March 15th 2016 period. Four major advances have been achieved:
1. See-through-wall Radar technique has been first developed and evaluated in the flow reactor. In situ, see-through-wall measurements of rotational temperature of molecular oxygen have been demonstrated using Radar Resonance Enhanced Multiphoton Ionization (REMPI) in a quartz flow reactor at atmospheric pressure. Both axial and radial temperature distributions of heated air in flow reactor have been obtained and the results have been verified by computational model. See-through-wall Radar technique shows its prestige on species detection (i.e., molecules and radicals) with high spatial resolution and in situ measurement results.

**15. SUBJECT TERMS**
Combustion, diagnostics, rempi

| 16. SECURITY CLASSIFICATION OF: | | | 17. LIMITATION OF ABSTRACT | 18. NUMBER OF PAGES | 19a. NAME OF RESPONSIBLE PERSON |
|---|---|---|---|---|---|
| a. REPORT | b. ABSTRACT | c. THIS PAGE | | | LI, CHIPING |
| Unclassified | Unclassified | Unclassified | UU | | 19b. TELEPHONE NUMBER *(Include area code)* 703-696-8574 |

Standard Form 298 (Rev. 8/98)
Prescribed by ANSI Std. Z39.18

# Final Report

# Preliminary Work for Identifying and Tracking Combustion Reaction Pathways by Coherent Microwave Mapping of Photoelectrons

Contract No. FA9550-14-1-0329

Submitted to

Program Manager: Dr. Chiping Li

Energy and Combustion Sciences
AFOSR

by

PI: Prof. Zhili Zhang
University of Tennessee Knoxville

**June 13, 2016**

## Abstract

This report summarizes our efforts during Sep. 15th 2014 – March 15th 2016 period. Four major advances have been achieved:

1. *See-through-wall* Radar technique has been first developed and evaluated in the flow reactor. In situ, *see-through-wall* measurements of rotational temperature of molecular oxygen have been demonstrated using Radar Resonance Enhanced Multiphoton Ionization (REMPI) in a quartz flow reactor at atmospheric pressure. Both axial and radial temperature distributions of heated air in flow reactor have been obtained and the results have been verified by computational model. *See-through-wall* Radar technique shows its prestige on species detection (i.e., molecules and radicals) with high spatial resolution and in situ measurement results.
2. New flow reactors collaborated with *see-through-wall* Radar technique has been built and preliminary results of pyrolysis of iso-butane have been obtained. Qualitative measurements of ethylene in pyrolysis products have been conducted by using coherent microwave Rayleigh scattering (Radar) from Resonance Enhanced Multi-Photon Ionization (REMPI). The (2+1) REMPI ionizations of ethylene ($C_2H_4$, $1^1B_{3u}(\pi,3p)$ Rydberg manifold) was selectively induced at 310─325nm. The ethylene was detectable at 1 ppm in the quartz cell with the spectrum being confirmed. Measurements in the flow reactors were conducted.
3. New high-pressure combustion chamber has been built. Measurements of atomic oxygen concentration have been measured at pressures up to 5 bar. New quantitative measurements provide new tools for combustion diagnostics.
4. New laser ignition methods have been demonstrated for high-pressure combustion. By utilizing high-power high repetition rate laser, we have demonstrated that an order of magnitude lower individual laser pulses can successfully ignite the fuel/air mixture.

New absorption based measurement and single-shot temperature measurement techniques are being developed for simultaneous temperature and multiple species measurements in the pyrolysis processes. It will be reported in the next report. In this annual report, we demonstrate temperature measurement with spatial distribution in a flow reactor. The species detection and measurement with spatial resolution have been designed and will be fulfilled in the near future.

## Description

The proposed research seeks to develop novel diagnostic techniques for combustion kinetics chemistry development, with focus of initial breakups of fuel molecules. The goal is to *in situ* identify and track key rate-controlling reaction pathways in the combustion by using advanced microwave and laser diagnostics techniques. Compared to the conventional analysis methods, we demonstrated see-through-wall technique by using microwave source as the detection tool which can penetrate normal heat component of the flow reactor. Hence, in-situ measurement of chemical species occurring in the pyrolysis process is available, which could provide detail information inside the reactor and improve the understanding of fuel breakups, pyrolysis and slow oxidation processes happening inside the reactor. In this annual report, spatial (axial and radial) scanning of temperature distribution has been demonstrated in a flow reactor with error less than 5% and ± 20 K uncertainty. Such technique proves its capability to conduct in situ measurement inside the reactor rather than analyzing products streaming out from the reactor. The pyrolysis of iso-butane has been first demonstrated in a new designed flow reactor with the quantitative measurements of ethylene as one of the pyrolysis products by using coherent microwave Rayleigh scattering (Radar) from Resonant Enhanced Multi-photon Ionization (REMPI). The (2+1) REMPI ionizations of ethylene ($C_2H_4$, $1^1B_{3u}(\pi,3p)$ Rydberg manifold) was selectively induced at 310 – 325 nm. The ethylene was detectable at 1 ppm in the quartz cell with the spectrum being confirmed. Beside the study of pyrolysis process in the flow reactor with low-pressure environment, the high pressure chamber has been built as well to extend the combustion study in a real and practical environment. (a) Measurements of atomic oxygen concentration have been measured at pressures up to 5 bar. (b) New laser ignition methods have been demonstrated for high-pressure combustion. By utilizing high-power high repetition rate laser, we have demonstrated that an order of magnitude lower individual laser pulses can successfully ignite the fuel/air mixture. Some work was conducted through collaborations with Dr. James Gord and Dr. Sukesh Roy at Wright Patterson Air Force base.

Specifically, we demonstrated the following tasks for the preliminary work:

### Task 1: *See-through-wall* temperature mapping in a flow reactor

The initial breakups and oxidation of fuel molecules in flow reactor are sensitive to the temperature map provided by the surrounding heat component. Even the flow reactor is well designed to offer uniform heat source for fuel breakups and oxidation processes, the fuel and oxidizer fluid mixture distribute a non-uniformed flow pattern. Especially near the boundary layer, the heat transfer is highly dependent on the molecule convection and cell surface radiation. Conventional flow reactors are limited by studying the products downstream outside the flow reactor by controlling the residence time, however, have weak knowledge about the local temperature, heat release and radical concentration inside the reactor. Hence, the see-through-wall Radar technique provides us an excellent access to explore the chemical reactions inside the reactor even with no optical access which is essential to all optical-based laser diagnostics. Here we demonstrate the rotation temperature measurement of molecular oxygen (oxidizer) inside a flow reactor with spatial temperature distribution in both axial and radial directions.

The concise experimental setup is shown in Fig. 1. A UV beam (284 nm ~ 289 nm) has been focused by a lens ($f$ = 150 mm) and used to detect molecular oxygen inside the flow reactor. Two cylindrical heat components have been applied to provide stable heat source for the reactor. The temperature is controlled at 675 K with fluctuation less than 1 K. The microwave detection system has been used to collection microwave signal from ionized oxygen through the heater insulation (ceramic fiber). The microwave horn is shown in the figure. Ambient air at room temperature (298 K) has been delivered into the cell from left to right (Fig. 1). The air flow rate is set at 2 standard liter per minute (slpm).

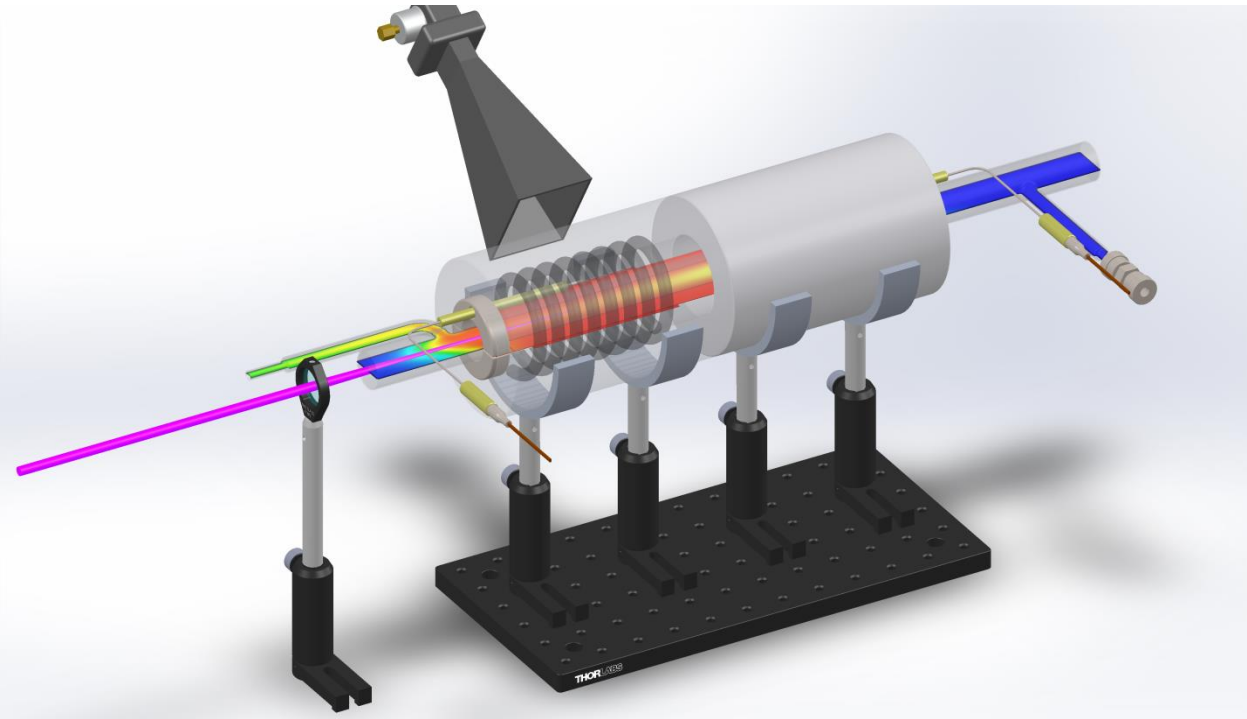

*Fig. 1. Experimental setup for see-through-wall temperature measurement of molecular oxygen in a flow reactor.*

The typical REMPI spectral finger prints are shown in Fig. 2(a) and 2(b). The blacklines are experimental results and red lines are simulation from $O_2$ REMPI model. With respect to the temperature variation, the overall shape of $O_2$ spectrum changes dramatically due to the molecule thermal dynamics. Hence Boltzmann plot method was applied to extract the temperature from the spectral information.

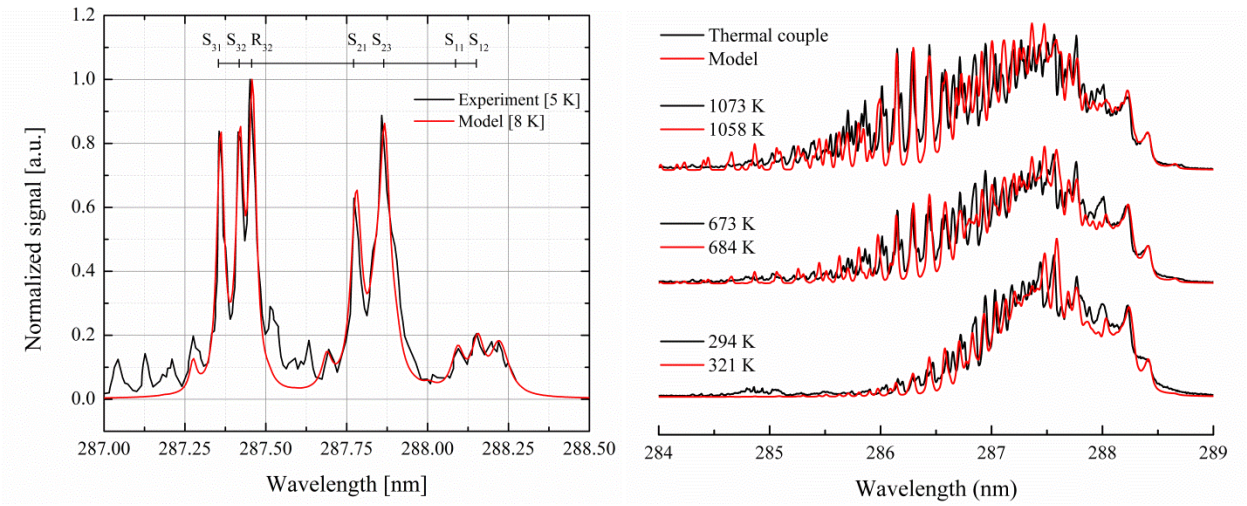


(a) (b)

*Fig. 2. The spectrum of molecular oxygen by using 2+1 REMPI process. (a) Spectrum obtained with ultra-low temperature (5 K); (b) Spectra obtained at room temperature and elevated temperature conditions (i.e., heated air in a flow reactor).*

Besides the unique characteristics, "see-through-wall", simple-and-robust are another key feature of Radar REMPI. Only one laser beam is required and it is simply focused by a focal lens. By using a 150-mm focal lens, the beam waist is around 100 μm with a few millimeters in length. Hence, the spatial scanning is capable for Radar REMPI to obtain the temperature/species map inside the flow reactor in both radial and axial directions.

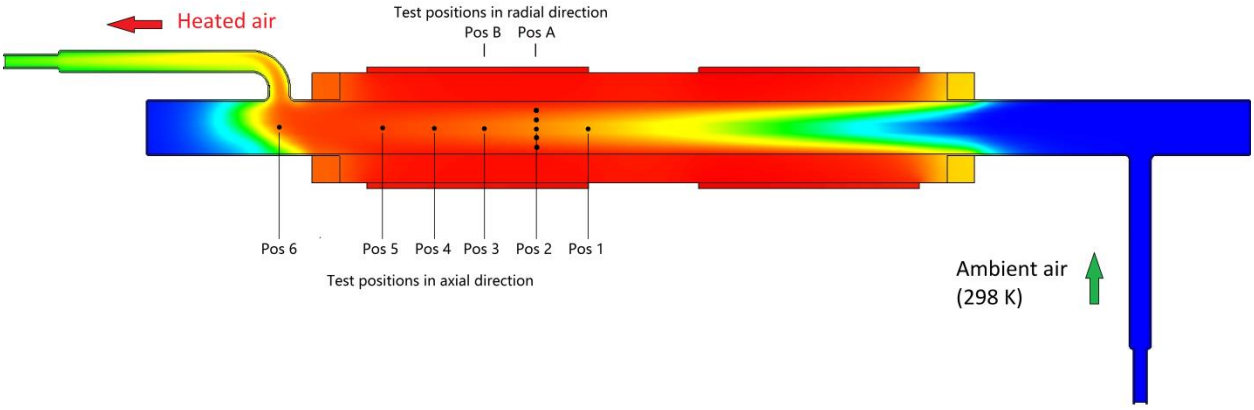


*Fig. 3. The computational result of the flow reactor heated by cylindrical heater. The black dots indicate the testing points for temperature measurements in both axial and radial directions.*

Oxygen in the $X^3\Sigma_g^-(v''=0)$ ground state is a bi-radical molecule showing paramagnetic behavior. The two unpaired electrons each have a spin state of 1/2 for total resultant spin S of 1, making ground state oxygen a triplet $(2s+1)=3$. The triplet ground state can be best described as Hund's case (b), and the term energy components of these three spin states can be expressed as $G_1$, $G_2$ and $G_3$ representing $J=N+1, N$ and $N+1$ respectively. These energy components for a specific $N$ value are determined as follows

$$G_1 = B_0N(N+1) - D_0N^2(N+1)^2 - \lambda + \gamma(N+1) \\ +B_0(2N+3) - [\lambda^2 - 2\lambda B_0 + B_0^2(2N+3)^2]^{1/2}$$

$$G_2 = B_0N(N+1) - D_0N^2(N+1)^2$$

$$G_3 = B_0N(N+1) - D_0N^2(N+1)^2 - \lambda - \gamma N \\ -B_0(2N-1) + [\lambda^2 - 2\lambda B_0 + B_0^2(2N-1)^2]^{1/2}.$$

The molecular constants, $B_0, D_0, \lambda$ and $\gamma$ have been previously tabulated for $O_2(X^3\Sigma_g^-(v''=0))$, where the rotational constant used here is $B_0 = 1.43768\ cm^{-1}$, the centrifugal distortion constant used is $D_0 = 4.790 \times 10^{-6}\ cm^{-1}$, the spin-spin coupling parameter used is $\lambda = 1.98475$ and the spin-rotation coupling parameter used is $\gamma = 0.008425\ cm^{-1}$.

Meanwhile, the intermediate level in our REMPI scheme, the $C^3\Pi_g$ Rydberg state of $O_2$, is a triplet as well, which is best described as Hund's case (a). It is found that the $C^3\Pi_g$ Rydberg state is generally very diffuse and has rotationally resolved structure for the $v' = 2$ level only. The term energies of $O_2(C^3\Pi_g(v'=2, J'))$ have been previously fitted by least squares to the following polynomials:

$$F_1 = n_{01} + B_{eff1}J'(J'+1) - D_{v1}J'^2(J'+1)^2,$$
$$F_2 = n_{02} + B_{eff2}J'(J'+1) - D_{v2}J'^2(J'+1)^2,$$
$$F_3 = n_{03} + B_{eff3}J'(J'+1) - D_{v3}J'^2(J'+1)^2,$$

where the empirically derived constants are listed in Table 1 based on the previous experimental and computational study of the REMPI spectra of $O_2$. The rotational-resolved hyperfine structures for this REMPI process can be determined by the energy difference of the allowed transitions between the triplet ground and Rydberg states. The two-photon rotational line strength parameter for each $C^3\Pi_g(v'=2, J') \leftarrow\leftarrow X^3\Sigma_g^-(v''=0, J'')$ transition line, is $T_{f,g}^{(2)}(J', J'')$ where the $g$ subscript denotes the ground $X^3\Sigma_g^-(v''=0)$ state and the $f$ subscript denotes the intermediate $C^3\Pi_g(v'=2)$ state. With these states having Hund's case (a) and case (b) coupling respectively, the rotational line strengths can be expressed as follows:

$$T_{f,g}^{(2)}(J', J'') = \sum_{k=0,2} \frac{\left|\beta_k^{(2)}\right|^2}{2k+1} \cdot (2J'+1) \cdot (2J''+1) \cdot (2N''+1) \\ \times \begin{bmatrix} J'' & S' & N'' \\ \Lambda''+\Sigma' & -\Sigma' & -\Lambda'' \end{bmatrix}^2 \begin{bmatrix} J' & k & J'' \\ \Omega' & -\Delta\Lambda & -\Lambda''-\Sigma' \end{bmatrix}^2,$$

where […] is the Wigner 3-j symbol, $J$ is the rotational quantum number, $N$ is total angular momentum except the spin, $\beta_k^{(2)}$ is polarization coefficient, double-primed parameters denote the ground state of $X^3\Sigma_g^-$ and primed parameters denote the Rydberg state of $C^3\Pi_g$. For this experiment with linearly polarized laser light, terms with $k = 0$ and 2 contribute to the final line strength, giving $\beta_k^{(2)} = \sqrt{10/3}$.

The homodyne transceiver detection system was utilized to collect the signal. The microwave scattering signal from the REMPI produced plasma is proportional to the total number of electrons inside the plasma, which is proportional to the total number of electron excitations to the continuum through the resonant two-photon transition followed by the single photon ionization. The total number of electron excitations to the continuum is thus determined by the product of the number of molecules in the ground state and the rate of multiphoton ionization. The resulting microwave scattering signal, $E_{MW}(J', J")$, for each two-photon transition line from $X^3\Sigma_g^-(v'' = 0, J'')$ state to $C^3\Pi_g(v' = 2, J')$ state can be determined by assuming that $E_{MW}(J', J'') \propto N_e(J', J'')$ where $N_e(J', J'')$ is the electron density in the REMPI induced plasma for a specific ro-vibronic transition. Then the microwave scattering signal can be written as

$$E_{MW}(J', J'') = N_o \cdot T_{f,g}^{(2)}(J', J'') \cdot I^2 \cdot T_{i,f}^{(1)} \cdot I \cdot \exp(-E_g(J'')/k_B T)$$

where $N_o$ is the total number of oxygen molecules in the laser focal region, $E_g(J'')$ is the rotational energy of the ground state $X^3\Sigma_g^-(v'' = 0, J'')$ level, $k_B$ is the Boltzmann constant, $T$ is the rotational temperature value, $I$ is the intensity of the laser beam, and $T_{i,f}^{(1)}$ is the ionization cross section from the intermediate state ($f$) to the ionization continuum ($i$).

The variation of the intensity of the rotational lines in an electronic manifold is determined by the thermal population distribution of the rotational levels. The rotational temperature can be extracted from the analysis of the rotational structures revealed in the REMPI spectra. The thermal distribution of the rotational levels is given by a statistically weighted (i.e. quantum degenerated) Boltzmann factor of $(2J + 1)\exp(-E_g/k_B T)$, where the rotational level with the maximum population shifts toward higher J values with increasing temperature. If $T_{fi}$ is assumed to be constant due to limited scanning range and the ground state population $N_0$ is constant during the scan time, then the Boltzmann plots can be formulated as

$$\frac{\log\left(\frac{E_{MW}}{I^3 T_{f,g}^{(2)}}\right)}{E_g} \propto -\frac{1}{k_B T}$$

when a region of the spectrum including numerous rotational lines is measured, a statistical fit of the Boltzmann plot gives an accurate representation of the rotational populations and thus the rotational temperature, i.e., the slope of the Boltzmann plot as shown in the equation above.

In this experiment, the $S_{21}$ branch of the REMPI rotational spectra has been used for the Boltzmann plots for temperature extraction. The Boltzmann plots are shown in Fig. 4.

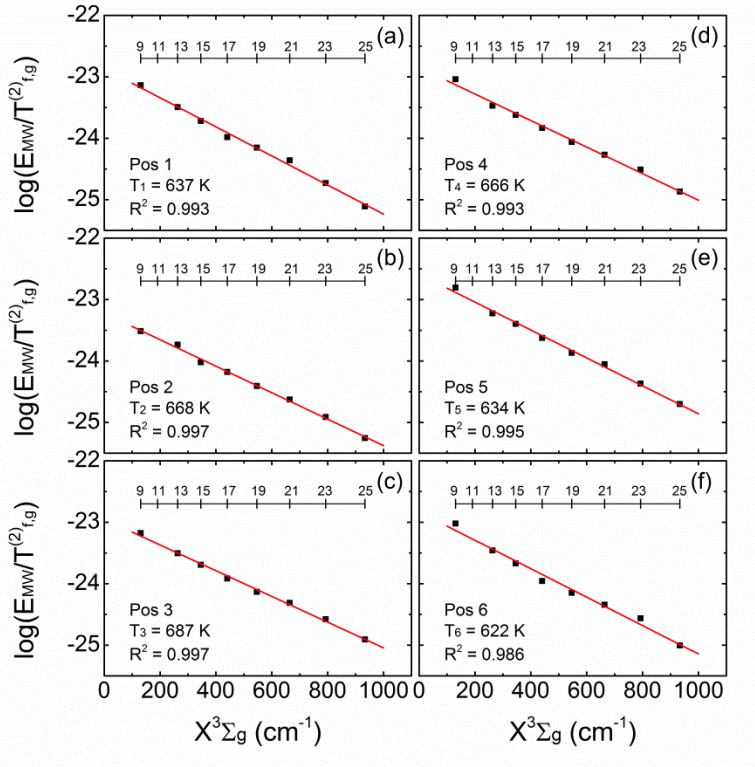


*Fig. 4. Boltzmann plots for oxygen temperature determination by rotational lines of $S_{21}(J''=9\sim25)$. Six testing points (Pos 1 – Pos 6 shown in Fig. 3) in axial direction have been set for temperature measurements.*

Based on the temperature extraction from Boltzmann plots, the temperature distributions are obtained in both axial and radial directions as shown in Fig. 5. The lines shown in Fig. 5 are computational results and the star points are the experimental results. As shown in Fig. 5(a), solid line offers the temperature distribution along the center line of the flow reactor. The temperature distribution indicates the existence of temperature gradient inside the flow reactor. Both dash and dot lines in Fig 5(a) provide extra temperature information near the center line with 0.2 inch offset in both sides. In the measurement, six points are tested with five of them located inside the reactor and the rest one is located downstream outside it which have been marked in Fig. 3.The radial scan for temperature distribution is even more attracted. Since the boundary lay and no slip effect exist near the inner surface of the flow reactor, the temperature distribution shows its unique feature which has been well predicted by the simulation. As close to the surface, the air temperature is heated up by surface conduction and radiation with the temperature near the setting point 675 K. However the heat radiation is much weaker in the center of the flow reactor and only the heat convection plays the key role for the heat transportation.

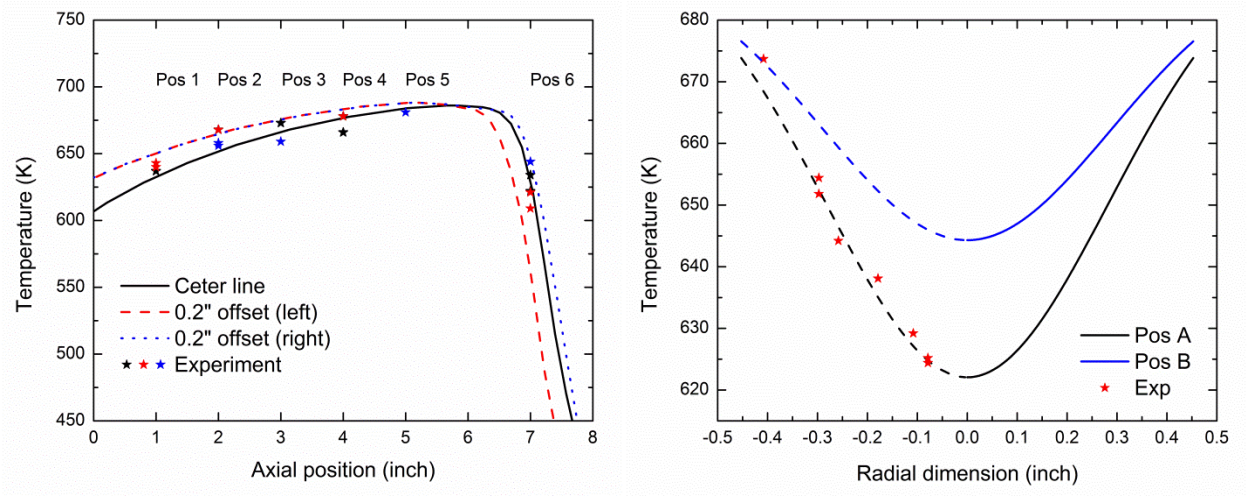


(a) (b)

*Fig. 5. The spatial distribution of $O_2$ rotational temperature in the flow reactor in both axial and radial directions.*

In this report, the ambient air heating and temperature measurements have been demonstrated in a flow reactor with both axial and radial spatial distributions with measurement error of less than 5% and uncertainty ± 20 K. With the "see-through-wall" ability, Radar REMPI shows its unique power to acquire the thermal information inside the flow reactor. The temperature variations and distribution ensure us better design the flow reactor and the residence time of fuel/oxidizer mixture.

Next step, single shot temperature calibration in flow reactor will be performed with continuous temperature measurement along the flow reactor in both heated air and fuel pyrolysis process.

**Task 2: Flow Reactor.** New flow reactors have been built and preliminary results of pyrolysis of butane and iso-butane have been obtained. Qualitative measurements of ethylene in pyrolysis have been conducted by using coherent microwave Rayleigh scattering (Radar) from Resonance Enhanced Multi-Photon Ionization (REMPI). The (2+1) REMPI ionizations of ethylene ($C_2H_4$, $1^1B_3u(\pi,3p)$ Rydberg manifold) was selectively induced at 310─325nm. The ethylene was detectable at 1 ppm in the quartz cell with the spectrum being confirmed. Preliminary measurements in the flow reactors were conducted.

Before directly measuring ethylene in the flow reactor, the detection limit of ethylene was first explored in the experiments in a quartz cell with the spectrum verified by the previous work [1]. Fig.6 shows the two-photon resonance enhanced excitation spectra of ethylene over ranges of 59000-68000 $cm^{-1}$. Due to the limitation of the power in the dye laser system, the ethylene was confirmed at the range of 62000-65500 $cm^{-1}$ and 66300-67600 $cm^{-1}$ by using two different dyes (i.e. Rhodamine 610 and DCM) separately. The experimental results have good agreement with the data of the reference [1] as shown in Fig. 6.

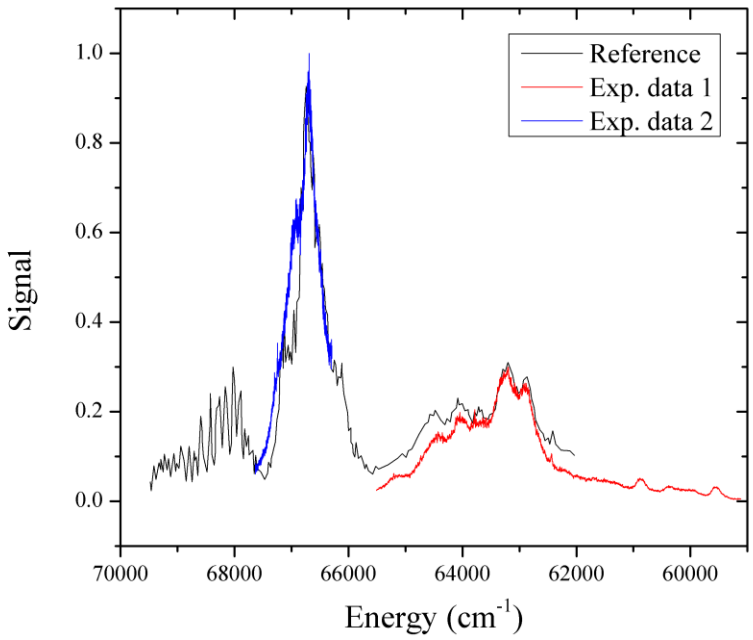


*Fig. 6. The spectra of ethylene obtained in a quartz cell by using (2+1) Radar REMPI from 59000-68000 cm$^{-1}$. The black line is the spectrum provided in the previous work. The red line and blue line are the experimental data obtained with the pure ethylene in the quartz cell at pressure of 100 Torr and room temperature.*

The detection limit of the Radar REMPI technique for the measurement of ethylene in the quartz cell was then conducted. The two-photon resonance enhanced excitation spectra of ethylene were separately scanned and recorded at the range of 66250-67625cm$^{-1}$ and 61750-64750 cm$^{-1}$ as shown in Fig. 7(a) and Fig. 7(b), respectively. As the experimental results shown in Fig. 7(a), the ethylene was detectable down to 1 ppm in $N_2$ buffer gas at 1000 Torr by using the Radar REMPI technique. Though the signal was decreased 5 times as the density of ethylene was diluted from $10^4$ ppm to 10 ppm, such signal-to-noise ratio is still acceptable for the spectrum scanning results.

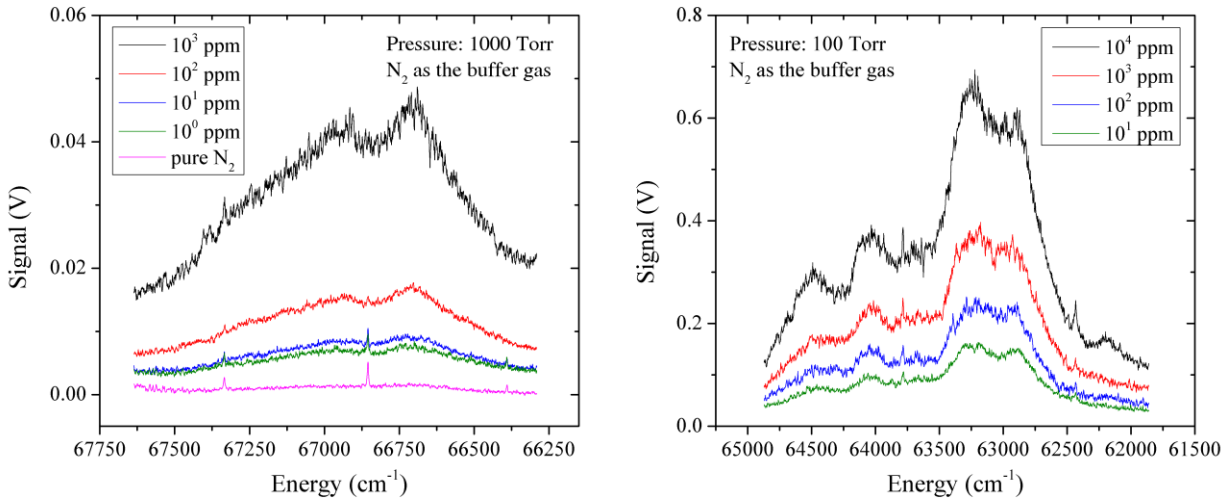


(a) (b)

*Fig. 7. The spectra of ethylene obtained in the quartz cell at room temperature with $N_2$ as the buffer gas. The density of ethylene was diluted from $10^4$ ppm to 1 ppm.*

Figure 8 shows the experimental setup of the new-designed flow reactor. The current flow reactor has two distinct features. First it can measure both stable and unstable species by nonintrusive optical diagnostic techniques. Second, it only requires single end window for the laser probing. The detection is done by see-through-the-wall microwave detection, which can penetrate the ceramic heaters. The two features provide a new capability for the kinetic development since it provides more calibration dimensions for various unstable species, which are usually not accurately measured in the flow reactor experiments. Additionally, the uniformity of the flow reactor can be insured which can provide more accuracy on the kinetic model development.

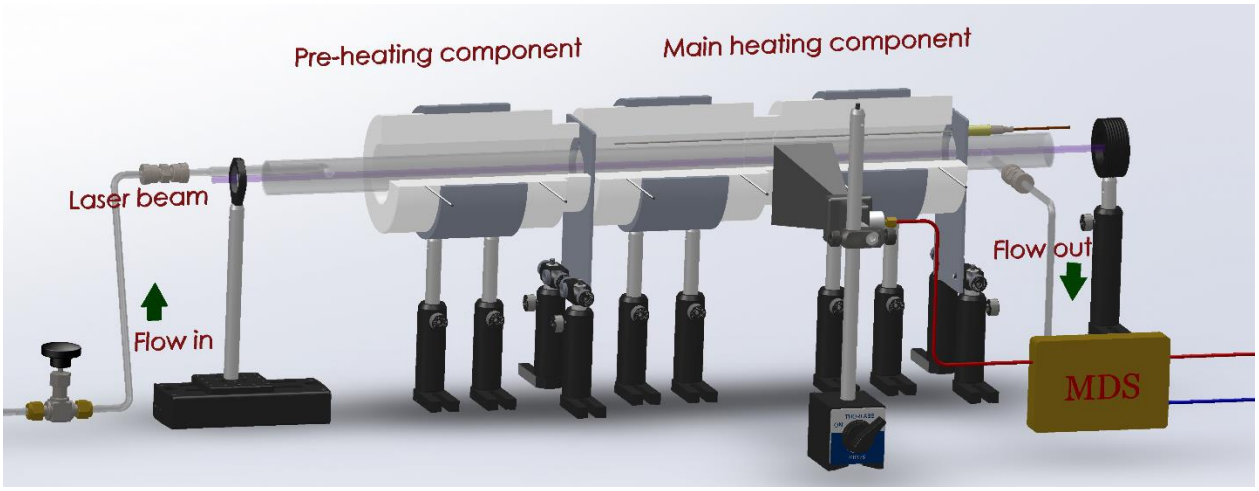


*Fig. 8. New flow reactor built at University of Tennessee*

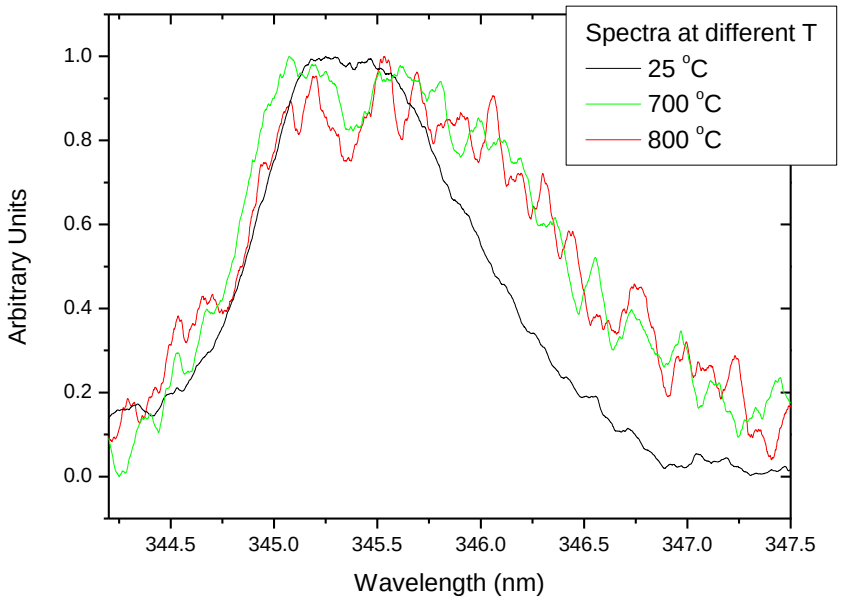


*Fig. 9. Normalized ethylene REMPI spectra at various temperatures out of the flow reactor.*

Figure 9 shows the normalized ethylene REMPI spectra. $C_2H_4$ is identified by matching the fine structures above the background with the reference spectrum. Concentration of pyrolysis is quantified by comparing with known flow conditions, i.e., calibration.

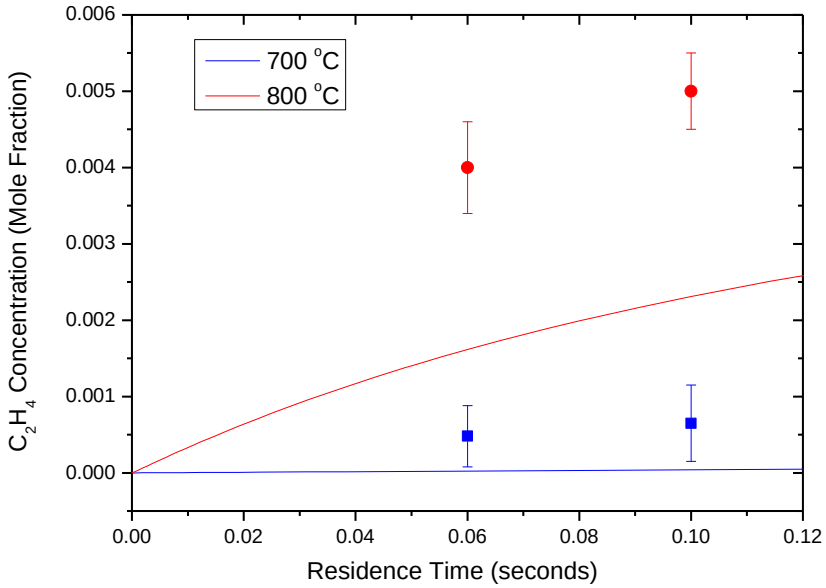

*Fig. 10. Comparison of preliminary measurements and kinetic modeling of ethylene in the flow reactor at various temperatures. Iso-butane at 0.5% is mixed with nitrogen, flowing through the flow reactor.*

Figure 10 show the preliminary results of the current measurements. Initial conditions are 0.5% butane ($C_4H_{10}$) in $N_2$ atmospheric pressure with residence time 0.05 – 0.1 second. Pyrolysis product was calibrated by flowing $C_2H_4$ at the same condition. Solid lines are from unoptimized USC II computation by Wenting Sun at George Tech. Large uncertainties lie in the current results.

More experiments are needed for quantitative and multi-scalar measurements of the pyrolysis products.

**Task 3: High Pressure Chamber.** New high-pressure combustion chamber has been built. Measurements of local fuel/air ratio and atomic oxygen concentration have been demonstrated at pressures up to 15 bar. New quantitative measurements provide new tools for combustion diagnostics.

The high-pressure combustion chamber with optical accesses was built by Prof. Zhili Zhang at University of Tennessee. The schematic drawing of the chamber is shown in Fig. 11. The inner chamber dimension is 5.85 inch diameter by 25 inch height. The chamber has four 2-inch diameter windows for optical diagnostics. The high-pressure chamber can accommodate a 2-inch diameter Hencken burner for the required LIBS and Raman FAR calibration tests. Exhaust of gases was operated via a nozzle on the top. Air was used as a buffer gas to help push the exhaust away from the flame while also maintaining overall pressure in the chamber. Flow rates of oxygen, methane, and air were all controlled by digital flow meters. At high-pressure conditions water condensation would occur within the chamber. To resolve this issue, flowing of buffer gas (air) is applied to prevent water vapor from collecting on the windows of the pressure chamber used during the measurements. We have pressurized methane/air flame up to 15 bar and verified that no pressure leak or water condensation on the windows. The flame emission from the Hencken burner at pressure of 1, 5, 10, and 15 bar is shown in Fig. 12. The flame color becomes yellow at higher pressure resulting from soot generation.

one!for!fuel!and!one!

!

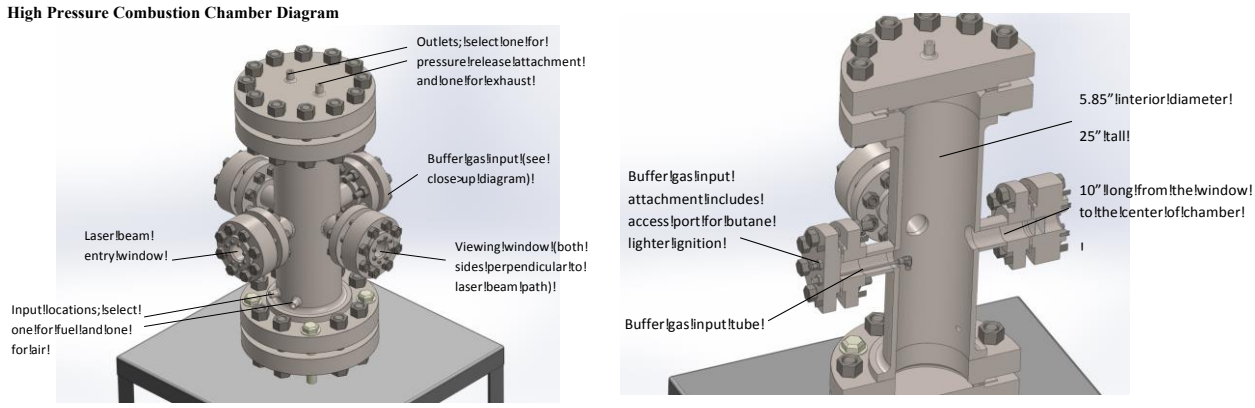


*Fig. 11. (Left) Schematic drawing of the high-pressure combustion chamber. (Right) Schematic diagram of a cross section of the chamber structure.*

25”!tall!

attachment!includes!

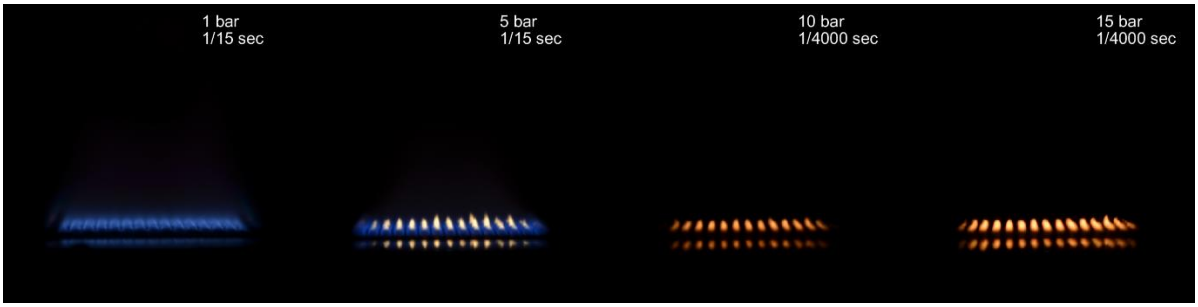


*Fig. 12. Methane/air flame of Hencken burner at various ambient pressures. The equivalence ratio was 1 for all cases. The flow rate was kept same at 0.8 slpm for methane and 10 slpm for air. At higher pressure, the mass flow rate was higher.*

Atomic oxygen was measured at elevated pressures in a Hencken flame. A frequency doubled Nd: YAG laser (Continuum Surelite SI-10) was used to pump a tunable dye laser (Continuum ND6000, DCM, [2-[2-[4-(dimethylamino)phenyl]ethenyl]-6-methyl-4H- pyran-4-ylidene]-propanedinitrile, $C_{19}H_{17}N_3O$ as the dye) to generate output at 619 nm. The output wavelengths were tunable from 615 to 620 nm, with output power ranging from 10-20 mJ/pulse. The dye laser output is mixed with the 355 nm beam (in BBO) to generate the required UV wavelength of 225 nm. The 225 nm UV beam, with energy per pulse of 50 μJ – 2mJ. The laser output was then focused by a lens with a focal length of 50 cm to generate the REMPI plasma in the methane/air flame of a Hencken burner in open air. A lens with a long focal length (50 cm) was used to avoid gas breakdown or avalanche ionization in the flame. From Gaussian beam geometry, the focal region was about 20 μm in diameter and 2.4 ± 0.4 mm in length. The length of the interrogation region arose from the microwave signal scattering along the laser beam upstream and downstream of the focus. The length and uncertainty was related to the laser intensity and corresponding microwave scattering

signal. At 2.8 mm, the laser intensity falls to about 33% and the REMPI efficiency and microwave scattering drop to about 11%, compared to the center of the laser focus. The beam steering mirrors and focusing lens were placed on a translational stage to move the laser focus through the flame front.

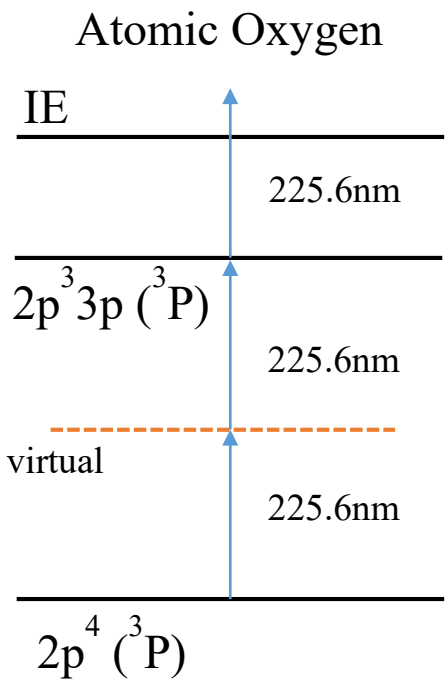


*Fig. 13. Energy level diagram for atomic oxygen measurement in the flame.*

Figure 14 shows a typical REMPI spectrum of atomic O in a methane/air flame at atmospheric pressure. The spectrum obtained in the flame was in agreement with previously published spectra. The measurement was conducted at 15 mm above the burner surface.

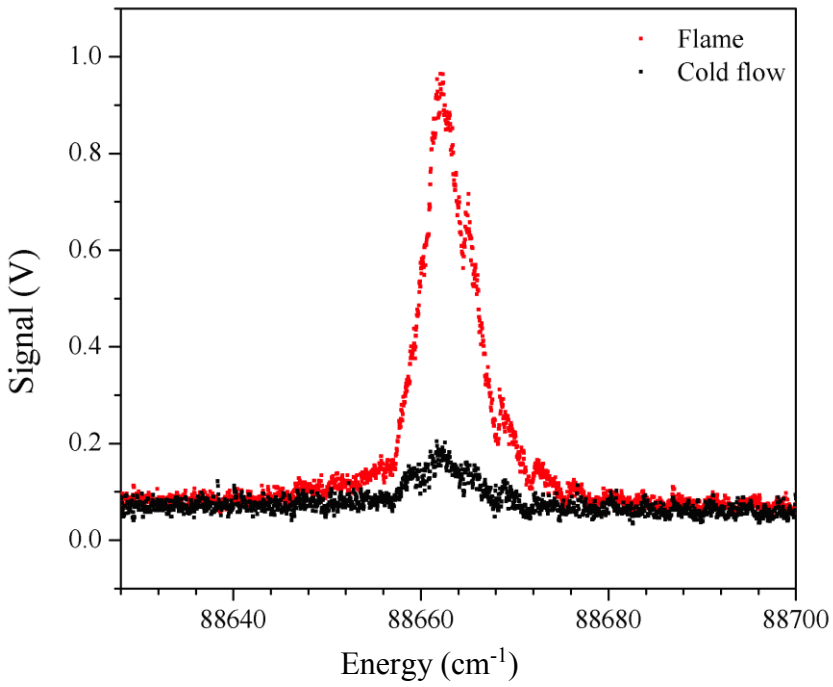


*Fig. 14. Atomic oxygen spectrum in the methane/air flame, with comparison with cold flow. The photolysis of molecular oxygen generates the atomic oxygen in the cold flow.*

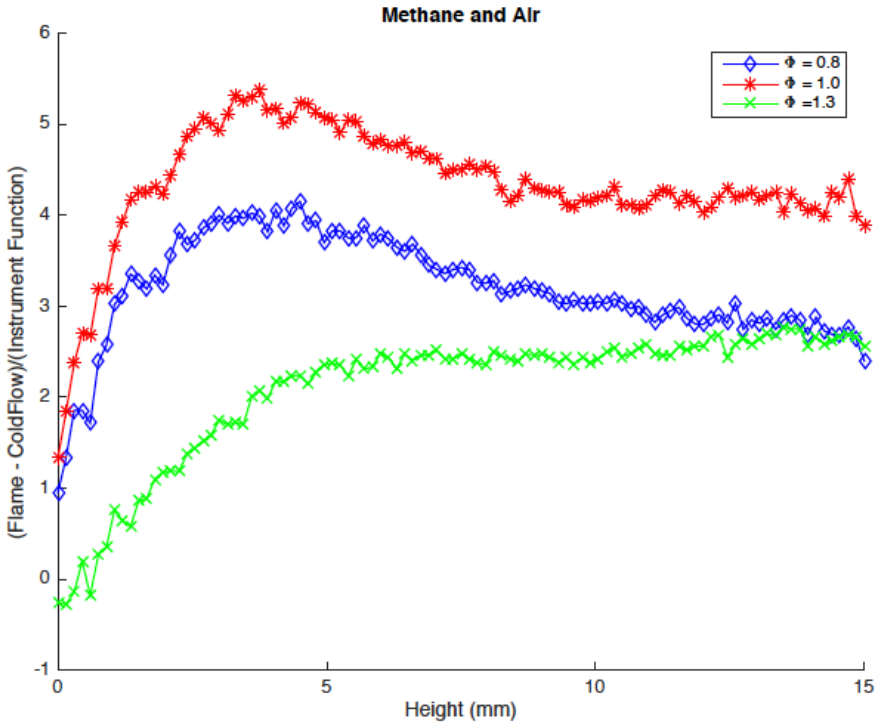


*Fig. 15. 1D concentration of atomic oxygen in atmospheric methane/air flame*

Figure 15 shows a typical 1D measurement of the atomic oxygen in the atmospheric methane/air flame. Within the high-pressure chamber, the $CH_4$/air flame was set at 4 bar pressure condition. By the same experimental setup, atomic oxygen has been successfully detected with the spectrum shown in Fig. 16. There is no photolysis effect in air at elevated pressure condition.

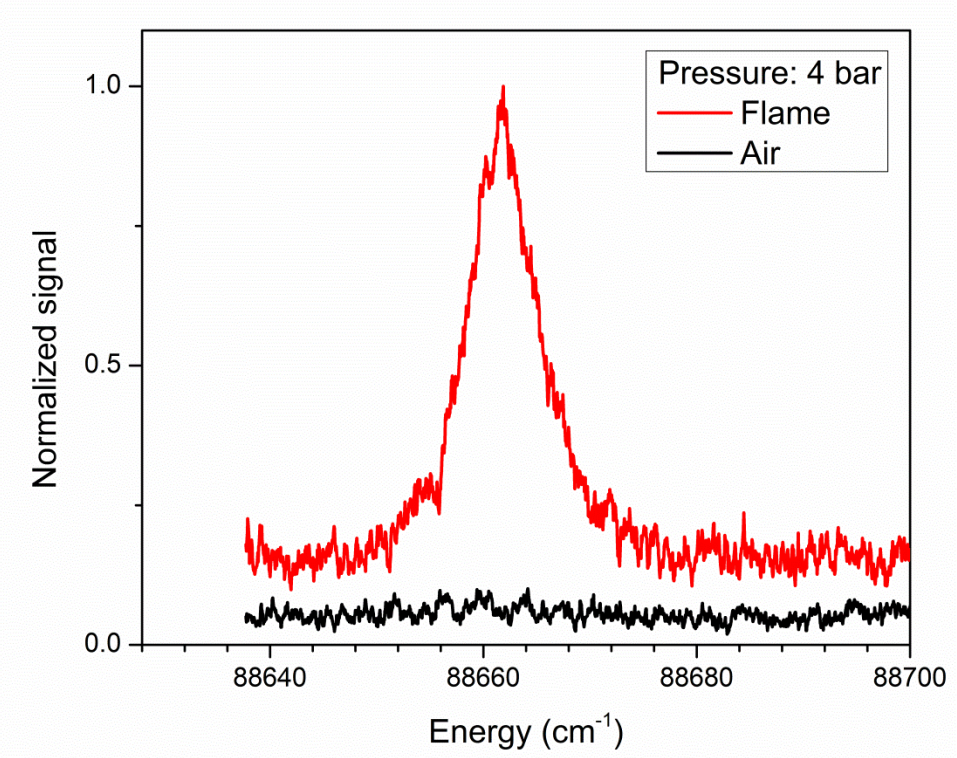


*Fig. 16. The atomic oxygen spectrum obtained in $CH_4$/air flame at elevated pressure condition (i.e., 4 bar). No photolysis effect has been found in air (black line).*

**Task 4:** New laser ignition methods have been demonstrated for high-pressure combustion. By utilizing high-power high repetition rate laser, we have demonstrated that an order of magnitude lower individual laser pulses can successfully ignite the fuel/air mixture.

We demonstrated that LI of combustible gaseous mixtures can be achieved with an order-of-magnitude reduction in per-pulse energy using a high-repetition-rate (HRR) nanosecond (ns)-laser pulse train. The HRR (10-100 kHz)-laser pulse train induces weakly ionized plasma typically within the first few pulses. The subsequent laser pulses enhance the plasma through energy deposition, which lead to sustained ignition. Generally, this approach can be viewed as an extension of the dual-pulse technique, with the number of pulses being easily varied from a few to multiples of tens. The HRR LI approach also increases the ignition probability of lean combustible mixtures in high-speed flows while maintaining low individual pulse energies.

Figure 17 displays the experimental setup used for laser ignition of iso-butane/air and ethylene/air pre-mixed flows that are output from a Hencken burner at atmospheric pressure. Iso-butane and ethylene fuels are commonly used for hypersonic wind tunnels and propulsion devices. The HRR pulses are generated from a Nd:YAG-based burst-mode laser (Quasimodo, Spectral Energies)]. The second harmonic of the burst-mode laser generated 10-ns laser pulses at various repetition rates (10 kHz-100 kHz). The laser beam was focused to the center of the Hencken burner using a spherical lens with a focal length of $f$ = 50 mm. The beam waist at the focal point was measured by a beam profiler (Spiricon, LW230); the typical beam waist at the focus was ~60 µm. For understanding the laser-plasma interaction during the laser ignition process, the generated plasma (i.e., free electrons) was detected by coherent microwave scattering. Additionally, a high-speed camera (Photron SA-Z) equipped with an intensifier (LaVision IRO) was used to track the chemiluminescence from OH*. The chemiluminescence was collected around 310 nm with a Cerco UV 45-mm, f⁄1.8 lens. A narrow bandpass interference filter (Semrock, FF02-320/40-25) was placed on the imaging lens. OH* chemiluminescence was utilized to identify the flame reaction zone and capture the flame front and propagation. The 2-D OH* chemiluminescence images were acquired with ~2 µs exposure time. Ignition delays and reaction times can be determined from the same measurements.

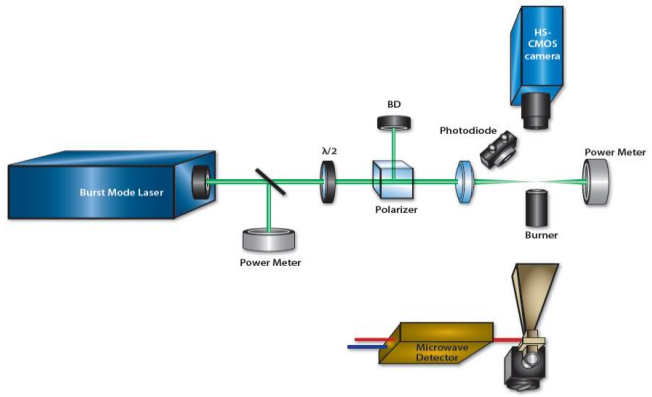


*Fig. 17. Schematic view of the experimental setup for laser ignition in Hencken burner.*

Figure 18 shows the coherent microwave scattering from an ionized laser-induced plasma formed in air using a 10-kHz pulse train. This demonstration is to show that multiple pulses from HRR laser can produce, sustain, and grow plasma. As shown in the Fig.18 the first pulse was used to generate the weakly ionized plasma, which acts as a gain medium for further energy deposition through inverse-bremsstrahlung and avalanche ionization processes by the following pulses. Because the overall plasma lifetimes at atmospheric pressure is ~100 ps and longer than the temporal spacing of the 10-kHz pulse train, the initial weak plasma is greatly enhanced by the subsequent pulses. This enhancement is shown by the increase in the microwave peaks with superimposed oscillations over the time span of the pulse train. Since the plasma generation near the laser breakdown threshold is stochastic due to many factors, the signals highly nonuniform, which corresponds to an unstable weakly ionized plasma though the laser pulses are uniform. Through thermalization process, enhanced plasma (i.e., hot electron) can transfer its thermal

energy to the ambient gases, eventually leading to localized thermal runaway and ignition in a combustible mixture, as shown in Fig. 18.

Figure 18 displays a comparison of laser ignition in a combustible mixture using a single pulse (i.e., 10-Hz laser) and HRR pulses [i.e., pulse repetition rate (PRR) of 10 kHz and 20 kHz]. This figure shows the temporally resolved images of OH* chemiluminescence from a typical ignition of an iso-butane/air mixture above a Hencken burner using a standard 10-Hz laser and the burst-mode laser operated at a 10-kHz and 20-kHz repetition rate. The flow and beam conditions (i.e., focused beam diameter, fuel/air mixture, and flow rate) are consistent for all three cases. The pulse energy used for ignition for the 10-Hz laser, 10-kHz laser, and 20-kHz laser was ~30 mJ/pulse, ~3.2 mJ/pulse, and ~2.8 mJ/pulse, respectively. For 10-Hz laser ignition, a high per-pulse energy is required to generate a plasma (bright emission spot shown in 10-Hz figure) for heating the surrounding fuel/air mixture and initiating the ignition process. It was found that the hot plasma is rapidly quenched within ~0.1 ms. The third through fifth images show a flame-front evolution that is very similar to that of a typical outwardly propagating spherical flame created by point spark ignition [1]. For 10-kHz and 20-kHz laser ignition, each pulse energy is ~10 times weaker than that used for 10-Hz laser ignition. We have verified that with a 10-Hz laser, the pulse energy <20 mJ/pulse generates the ionized plasma but not dense enough to initiate the ignition process. The emission from the plasma created by the low-energy laser pulse is weak; therefore, after attenuation by the OH* band-pass filter, the emission cannot be detected by the intensified camera. For the 10-kHz and 20-kHz cases, it was observed that the mixture was built up to a stable plasma after three to four consecutive laser pulses. Once the plasma was created, the subsequent HRR

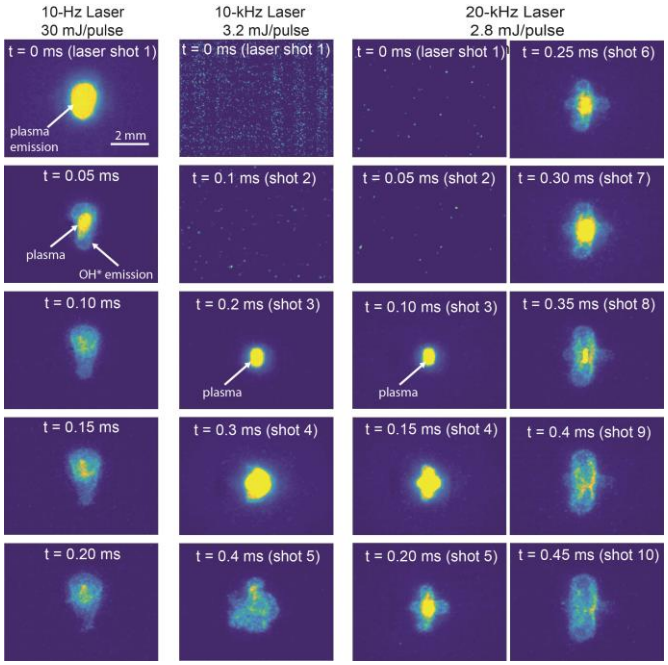


*Fig. 18. Laser ignition in iso-butane/air mixture at equivalence ratio $\phi = 1$ using 10-Hz laser (single laser shot) and HRR laser (10-kHz and 20-kHz repetition rate). Ignition-core evolution in iso-butane/air mixture above Hencken burner tracked by monitoring OH* chemiluminescence (Complete LI movies see also Media 1-3).*

laser pulses could keep depositing energies to sustain and grow the hot plasma for flame initiation and propagation. The lifetime of the plasma was characterized by strong emissions detected by the intensified camera. The ignition delays for the 10-kHz and 20-kHz laser are ~0.2 ms and ~0.3 ms, respectively. Extension of the hot-plasma lifetime can lead to a higher ignition success rate. For all of the cases, the premixed flame finally stabilized on the burner surface after ~7 ms.

Figure 19(a) shows minimum ignition energy (MIE) as a function of pulse repetition frequency for the ignition of iso-butane/air mixtures with equivalence ratio = 1 at atmospheric pressure. It should be noted that (i) MIE is defined as the minimal laser energy required to ignite the gas mixture with a probability of >50% and (ii) the comparison of MIE values in this work was conducted at the same focusing condition. At 10 Hz the ns lasers have a high MIE of ~30 mJ/pulse. It is observed that MIE decreases with an increase in PRR. When PRR increases from 10 Hz to 10 kHz, MIE decreases by an order of magnitude. Particularly, the MIE decreases ~10-12 times for PRR in the range 10 kHz -100 kHz. The required total energy for ignition is reduced by approximately a factor of two for HRR LI as compared to 10-Hz LI. We also noticed that the laser-energy absorption by plasma increases from ~12% to ~40% when PRR increases from 10 Hz to 10 kHz (both 10 Hz and 10kHz case incident laser energy is at ~3 mJ/pulse). This indicates that the HRR LI approach deposits laser energy to the plasma more efficiently. Because of the intensity threshold of generating plasma through the non-resonant-breakdown process, the per-pulse energy cannot be decreased continuously with an increased PRR. Figure 19(b) shows that the HRR LI approach can maintain the same energy per pulse across a wide equivalence-ratio range (0.65 - 1.2, ethylene/air mixture). The energy per pulse decreases ~10 times for the HRR LI approach as compared to 10-Hz-pulsed LI. Similar per-pulse ignition energy for the 20-kHz and 50-kHz pulse was observed; the reason for this may be that without sufficient initial electron generation by front-running pulses, the subsequent pulses cannot deposit sufficient energy to compensate for the heat losses and, thus, induce ignition.

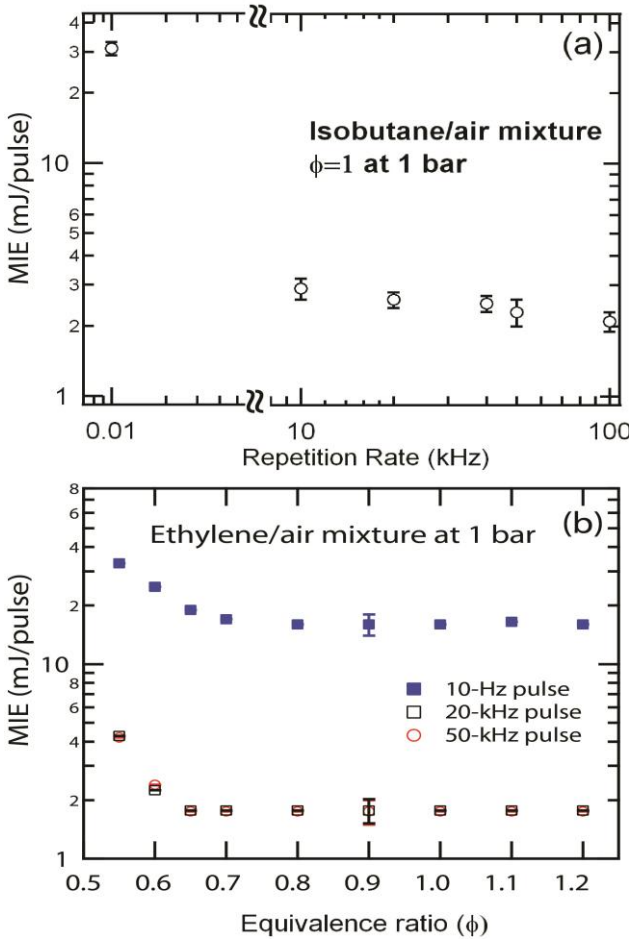


*Fig. 19 (a) MIE (input energy) as a function of repetition frequency. Iso-butane/air mixture of $\phi = 1$ at atmospheric pressure. (b) MIE as a function of equivalence ratio for ethylene/air mixture at atmospheric pressure. Burst duration for all HRR pulses is 0.5 ms.*

Publications during the period.

Archival Journal Papers

| |
|---|
| 1. Paul Hsu, Sukesh Roy, Zhili Zhang, Jordan Sawyer, Mikhail N. Slipchenko, Jason G. Mance, James R. Gord, "High-Repetition-Rate Laser Ignition of Fuel–Air Mixtures", Optics Letters, Vol. 41, Issue 7, pp.1570-1573, March 2016. doi: 10.1364/OL.41.001570S. |
| 2. Yue Wu, Zhili Zhang, Steven Adams, "Temperature sensitivity of molecular oxygen resonant-enhanced multiphoton ionization spectra involving the C3Πg intermediate state", Applied Physics B 122(5), 2016 DOI: 10.1007/s00340-016-6421-0 |
| 3. Yue Wu, Jordan C. Sawyer, Liu Su, and Zhili Zhang, "Quantitative measurement of electron number in nanosecond and picosecond laser-induced air breakdown", Journal of Applied Physics, **119**, 173303 (2016). DOI: 10.1063/1.4948431 |
| 4. Steven Adams, Yue Wu, Zhili Zhang, "O2 Rotational Temperature Determination by Empirical Analyses of C3Π(v′=2)←X3Σ(v′′=0) Transitions", Applied Spectroscopy, vol. 69, No.9, pp.1036-1041, 2015. |
| 5. Yue Wu, Zhili Zhang, "Two Dimensional Quantitative Measurements of Methyl Radicals in Methane/Air Flame", Applied Optics, Vol. 54, Issue 2, pp. 157-162, 2015. |
| 6. Jordan Sawyer, Jacques Abboud, Zhili Zhang, Steven F. Adams, "Reduction of Breakdown Threshold by Metal Nanoparticle Seeding in a DC Microdischarge", Nanoscale Research Letters, vol. 10, No. 15, 2015. DOI:10.1186/s11671-014-0709-y. |
| 7. Xinyuan Chong, Jacques Abboud, Zhili Zhang, "Plasmonics Resonance Enhanced Active Photothermal Effects of Aluminum and Iron Nanoparticles", Journal of Nanoscience and Nanotechnology, vol. 15, No. 3, pp. 2234-2240(7), 2015. DOI: 10.1166/jnn.2015.9698 |

Conference Papers

| |
|---|
| Liu Su, Yue Wu, Jordan C. Sawyer, Zhili Zhang, Quantitative Measurements of Electron Number Density and Threshold for Laser Induced Breakdown in Air (AIAA 2015-2964), 46th AIAA Plasmadynamics and Lasers Conference, 2015, 10.2514/6.2015-2964 |
| Yue Wu, Zhili Zhang, In situ Measurements of Ethylene and Methyl Radical by using the Radar REMPI technique (AIAA 2015-0534), 53rd AIAA Aerospace Sciences Meeting, 2015, 10.2514/6.2015-0534 |

| |
|---|
| Jordan C. Sawyer, Jacques Abboud, Zhili Zhang, Steven Adams, Reducing the Breakdown Threshold in DC Microdischarges via Metal Nanoparticle Seeding (AIAA 2015-1388), 53rd AIAA Aerospace Sciences Meeting, 2015, 10.2514/6.2015-1388 |
| Liu Su, Yue Wu, Jordan C. Sawyer, Zhili Zhang, Quantitative Measurements of Electron Number Density and Threshold for Laser Induced Breakdown in Air (AIAA 2015-2964), 46th AIAA Plasmadynamics and Lasers Conference, 2015, 10.2514/6.2015-2964 |

1.

**1. Report Type**

Final Report

**Primary Contact E-mail**

**Contact email if there is a problem with the report.**

zzhang24@utk.edu

**Primary Contact Phone Number**

**Contact phone number if there is a problem with the report**

8652585678

**Organization / Institution name**

University of Tennessee Knoxville

**Grant/Contract Title**

**The full title of the funded effort.**

Combustion Reaction Pathways by Coherent Microwave Mapping of Photoelectrons

**Grant/Contract Number**

**AFOSR assigned control number. It must begin with "FA9550" or "F49620" or "FA2386".**

FA9550-14-1-0329

**Principal Investigator Name**

**The full name of the principal investigator on the grant or contract.**

Zhili Zhang

**Program Manager**

**The AFOSR Program Manager currently assigned to the award**

Chiping Li

**Reporting Period Start Date**

09/15/2014

**Reporting Period End Date**

03/15/2016

**Abstract**

This report summarizes our efforts during Sep. 15th 2014 – March 15th 2016 period. Four major advances have been achieved:

1. See-through-wall Radar technique has been first developed and evaluated in the flow reactor. In situ, see-through-wall measurements of rotational temperature of molecular oxygen have been demonstrated using Radar Resonance Enhanced Multiphoton Ionization (REMPI) in a quartz flow reactor at atmospheric pressure. Both axial and radial temperature distributions of heated air in flow reactor have been obtained and the results have been verified by computational model. See-through-wall Radar technique shows its prestige on species detection (i.e., molecules and radicals) with high spatial resolution and in situ measurement results.

2. New flow reactors collaborated with see-through-wall Radar technique has been built and preliminary results of pyrolysis of iso-butane have been obtained. Qualitative measurements of ethylene in pyrolysis products have been conducted by using coherent microwave Rayleigh scattering (Radar) from Resonance Enhanced Multi-Photon Ionization (REMPI). The (2+1) REMPI ionizations of ethylene ($C_2H_4$, $1^1B_{3u}(\pi,3p)$ Rydberg manifold) was selectively induced at 310–325nm. The ethylene was detectable at 1 ppm in the quartz cell with the spectrum being confirmed. Measurements in the flow reactors were conducted.

3. New high-pressure combustion chamber has been built. Measurements of atomic oxygen concentration

have been measured at pressures up to 5 bar. New quantitative measurements provide new tools for combustion diagnostics.

4. New laser ignition methods have been demonstrated for high-pressure combustion. By utilizing high-power high repetition rate laser, we have demonstrated that an order of magnitude lower individual laser pulses can successfully ignite the fuel/air mixture.

New absorption based measurement and single-shot temperature measurement techniques are being developed for simultaneous temperature and multiple species measurements in the pyrolysis processes. It will be reported in the next report. In this annual report, we demonstrate temperature measurement with spatial distribution in a flow reactor. The species detection and measurement with spatial resolution have been designed and will be fulfilled in the near future.

**Distribution Statement**

**This is block 12 on the SF298 form.**

Distribution A - Approved for Public Release

**Explanation for Distribution Statement**

**If this is not approved for public release, please provide a short explanation. E.g., contains proprietary information.**

**SF298 Form**

**Please attach your SF298 form. A blank SF298 can be found here. Please do not password protect or secure the PDF The maximum file size for an SF298 is 50MB.**

AFD-070820-035 - Copy.pdf

**Upload the Report Document. File must be a PDF. Please do not password protect or secure the PDF . The maximum file size for the Report Document is 50MB.**

Flnal Report.pdf

**Upload a Report Document, if any. The maximum file size for the Report Document is 50MB.**

**Archival Publications (published) during reporting period:**

**2. New discoveries, inventions, or patent disclosures:**
**Do you have any discoveries, inventions, or patent disclosures to report for this period?**

No

**Please describe and include any notable dates**

**Do you plan to pursue a claim for personal or organizational intellectual property?**

**Changes in research objectives (if any):**

**Change in AFOSR Program Manager, if any:**

**Extensions granted or milestones slipped, if any:**

**AFOSR LRIR Number**

**LRIR Title**

**Reporting Period**

**Laboratory Task Manager**

**Program Officer**

**Research Objectives**

**Technical Summary**

**Funding Summary by Cost Category (by FY, $K)**

| | Starting FY | FY+1 | FY+2 |
|---|---|---|---|
| Salary | | | |
| Equipment/Facilities | | | |
| Supplies | | | |
| Total | | | |

**Report Document**

**Report Document - Text Analysis**

**Report Document - Text Analysis**

**Appendix Documents**

## 2. Thank You

**E-mail user**

Jun 13, 2016 06:43:45 Success: Email Sent to: zzhang24@utk.edu